Sensitivity analysis of fracture scattering

Xinding Fang[*], *Michael Fehler, Tianrun Chen and D.R. Burns, MIT Earth Resources Laboratory.*

Summary

The understanding of seismic scattering of a finite fracture is very important in reservoir fracture characterizations, but the analytical solution of this problem is not available. Thus, in this paper, we present an approach for numerical study of the seismic response of a finite fracture.

The way fractures affect seismic waves depends on fracture mechanical parameters, such as compliance and saturating fluid, and on their geometric properties, such as dimensions and spacing. When fractures are small relative to the seismic wavelength, waves will be weakly affected by fractures, and in effective medium theory, a zone comprised of many small fractures is equivalent to a homogeneous anisotropic zone without fractures (Hudson, 1991; Coates and Schoenberg, 1995; Schoenberg and Sayers, 1995; Grechka and Kachanov, 2006; Grechka, 2007; Sayers, 2009). When fractures are much larger than the seismic wavelength, then we can take fracture interfaces as infinite planes and apply plane wave theory to calculate their reflection and transmission coefficients and interface waves (Schoenberg, 1980; Pyrak-Nolte and Cook, 1987; Gu et al., 1996). In field reservoirs, fractures always have finite length, and fractures with characteristic lengths on the order of seismic wavelength are the scattering sources that generate seismic codas. Sanchez-Sesma and Iturraran-Viveros (2001) derived an approximate analytical solution of scattering and diffraction of SH waves by a finite fracture, and Chen (submitted 2010 SEG abstract) derived an analytical solution for scattering from a 2D elliptical crack in an isotropic acoustic medium. However, so far it is still difficult to derive the analytical elastic solution of a finite fracture with a linear-slip boundary and characteristic length on the order of the seismic wavelength. Although fractures are usually present as fracture networks in reservoirs, and the interaction between fracture networks and seismic waves is very complicated, scattering from a single fracture can be considered as the 1st order effect on the scattered wave field. Therefore, to study the general elastic response of single finite fracture is essential to reservoir fracture characterization, and this has been done numerically.

Here, we adopt Schoenberg's (1980) linear-slip fracture model and use the effective medium method (Coates and Schoenberg, 1995) for finite-difference modeling of fractures. In this model, a fracture is modeled as an interface across which the traction is taken to be continuous, yet displacement is allowed to be discontinuous. And the displacement discontinuity vector and the traction vector are linearly related by the fracture compliance matrix Z_{ij}. For a rotationally symmetric fracture, the fracture compliance matrix only has two independent components: the normal compliance Z_N and the tangential compliance Z_T.

Methodology

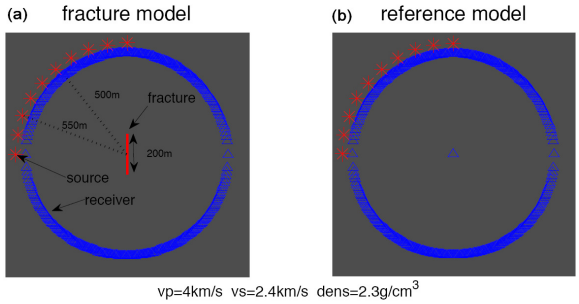

Figure 1: (a) is the fracture model and (b) is the reference model, these two models are exactly the same except for the presence of a fracture in (a) indicated by the red line. Blue triangles are receivers and they are equidistant from the fracture center, red asterisks indicate sources at different incident angles. Incident angles are measured from the normal of the fracture (e.g. a source directly above the fracture is considered to have a 90^0 incident angle).

As shown in figure 1, we recorded the wave fields in the fracture model (1a) and the reference model (1b). By subtracting the reference wave field from the wave field recorded in fracture model, we can obtain the scattered wave field, which is introduced by the fracture scattering. We assume the source is a pressure point source and we ignore the Earth's free surface, so the scattered wave field includes two parts: P-to-P scattered wave field $\mathbf{S_{pp}}$ and P-to-S scattered wave field $\mathbf{S_{ps}}$, which can be separated in an isotropic homogeneous media by simply calculating the divergence and curl of the scattered wave field. And we know that they also depend on incident angle.

$\mathbf{S_{pp}}$ and $\mathbf{S_{ps}}$ are frequency dependent, and we wish to obtain the fracture response function which is independent of the source pulse used in modeling.

Thus, in the frequency domain, we write

$$|\mathbf{S_{pp}}(\mathbf{r},\omega,\theta_{inc})|=F_{pp}(\theta,\omega)\bullet|\mathbf{I}(\omega,\theta_{inc})| \quad (1)$$

$$|\mathbf{S_{ps}}(\mathbf{r},\omega,\theta_{inc})|=F_{ps}(\theta,\omega)\bullet|\mathbf{I}(\omega,\theta_{inc})| \quad (2)$$

where $F_{pp}(\theta,\omega)$ and $F_{ps}(\theta,\omega)$ are P-to-P and P-to-S fracture response functions, respectively, and $\mathbf{I}(\omega,\theta_{inc})$ is the incident wave field recorded at the center of fracture, θ and θ_{inc} are scattering angle and incident angle, and ω is angular frequency.

Fracture scattering analysis

As mentioned above, $\mathbf{I}(\omega,\theta_{inc})$ is the incident wave field recorded at the center of the fracture, while $\mathbf{S_{pp}}(\mathbf{r},\omega,\theta_{inc})$ and $\mathbf{S_{ps}}(\mathbf{r},\omega,\theta_{inc})$ are the scattered wave field recorded at a certain distance away from the center of the fracture, as shown in figure 1, so we need to add a geometrical spreading factor in equations (1) and (2). Thus, the fracture response functions $F_{pp}(\theta,\omega)$ and $F_{ps}(\theta,\omega)$ can be expressed as

$$F_{pp}(\theta,\omega)=\frac{\left|S_{pp}(r,\omega,\theta_{inc})\right|}{a\left|I(\omega,\theta_{inc})\right|} \quad (3)$$

$$F_{ps}(\theta,\omega)=\frac{\left|S_{ps}(r,\omega,\theta_{inc})\right|}{a\left|I(\omega,\theta_{inc})\right|} \quad (4)$$

with

$$a=\begin{cases}1/\sqrt{r} & \text{for 2D}\\ 1/r & \text{for 3D}\end{cases}$$

is the geometrical spreading factor and r is the distance from the receiver to the fracture center.

Here, we emphasize that fracture response functions (3) and (4) are frequency dependent but are source-wavelet independent, we can get the same answer even though we use different source wavelets to calculate (3) and (4) numerically. $F_{pp}(\theta,\omega)$ and $F_{ps}(\theta,\omega)$ are functions of frequency, radiation angle, incident angle, matrix velocity, fracture compliance and wave-length to fracture-length ratio, and we can get the scattering radiation pattern by plotting them in polar coordinate.

Numerical Results & Discussions

(1) Fracture scattering pattern as a function of compliance.

From the comparison of many numerical results we find that, for a given incident angle, if we only consider the fracture response function as a function of fracture compliances (keep other conditions, such as background medium, fracture length, etc., unchanged), then the fracture scattering pattern is dominated by the compliance ratio γ ($\gamma=Z_N/Z_T$), and the scattering strength is affected by the magnitude of Z_N and Z_T.

Figure 2 shows the P-to-P fracture response functions of three different compliance ratios at four different incident angles. P-to-P fracture scattering patterns are nearly independent of compliance ratios when the incident angle is close to 0^0 or 90^0, while P-to-P back scattering changes significantly for different γ at intermediate incidence angles. Figure 3 shows the corresponding P-to-S fracture scattering patterns. P-to-S scattering patterns do not vary too much except for small angles of incidence, and in most cases P-to-S back scattering is much stronger than P-to-S forward scattering. For both P-to-P and P-to-S scattering, the scattering strength increases with increasing compliance magnitude, and the scattering pattern will not change if the compliance ratio does not change.

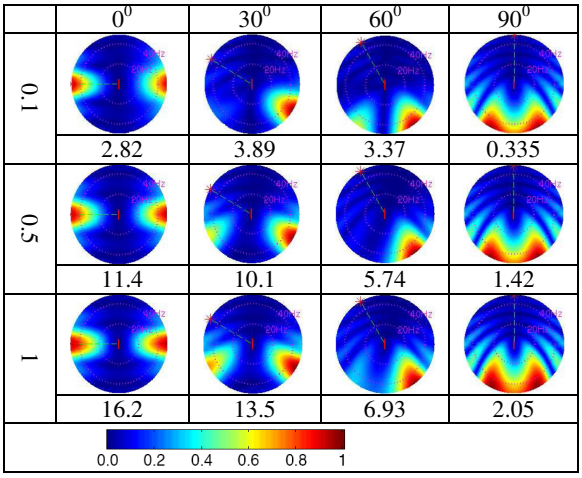

Figure 2: $F_{pp}(\theta,\omega)$ for different compliance ratio γ and different incident angles are plotted in polar coordinate, the radial and angular coordinates are $\omega/(2\pi)$ and θ. The range of $\omega/(2\pi)$ in each panel is from 0Hz to 50Hz. Incident angles, which are shown on top of the figure, are 0^0, 30^0, 60^0 and 90^0 for each column. The compliance ratio for each row is shown at the left side of each row. The number below each panel is the scaled factor in plotting and denotes the maximum scattering strength. Tangential compliance is fixed to 10^{-9}m/Pa, normal compliance varies. Fracture length is 200m, matrix P-wave and S-wave velocities are 4 km/s and 2.4 km/s, density is 2.3 g/cm^3.

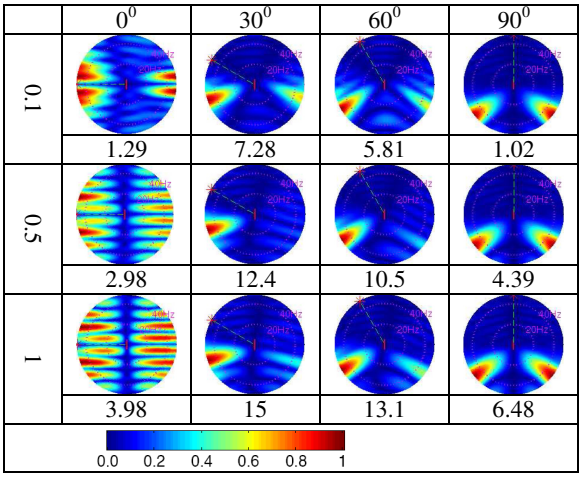

Figure 3: $F_{ps}(\theta,\omega)$ for different compliance ratio γ and different incident angles are plotted in polar coordinate, the radial and angular coordinates are $\omega/(2\pi)$ and θ.

Fracture scattering analysis

From figures 2 and 3, we can find that, when the incident angle is between 0^0 and 90^0, for P-to-P scattering, forward scattering is much stronger than back scattering, however, for P-to-S scattering, back scattering is much stronger than forward scattering. Moreover, most of the scattering energy propagates downwards if the fracture is close to vertical and the source is above the fracture. Specifically, the P-to-P scattering energy propagates down and forward (away from the source) while the P-to-S scattering energy propagates down and backward (towards the source). In the field, most fractures are close to vertical and the source is on surface. In this case, the seismic waves first will be diffracted by fracture tips, and then most of the scattering energy will propagate downward, and then it will be reflected back to surface by reflectors below the fracture zone, as illustrated in figure 4.

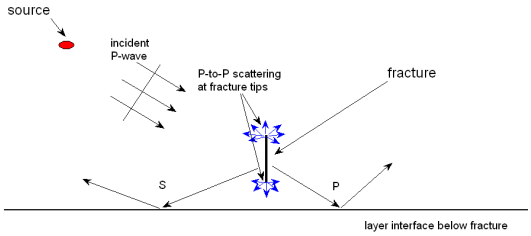

Figure 4: Cartoon showing how incident P-waves are scattered by a fracture. Scattering energy includes three parts: (i) P-to-P scattering at fracture tips; (ii) P-to-P forward scattering; (iii) P-to-S back scattering.

Figure 5 shows a numerical simulation of wave propagation in an uniform medium containing 21 non-parallel fractures, 5a shows the geometry of the model, 5b and 5c show snapshots of the divergent field and curl field of the scattered wave field at 0.54s (the scattered wave field is obtained by subtracting the whole wave field from the reference wave field of the same model without fractures). We can see that most of the P-to-P scattered energy is going down and forward and most of the P-to-S scattered energy is going down and backward. Therefore, most scattered signals observed on the surface come from fracture tips and reflectors below fracture zone. We can only see fracture tips if we use traditional migration methods to search for fractures. In order to image subsurface fractures, we need to develop statistical methods to analyze the fracture scattered signals, and the scattering index method (Willis, 2006) is one of these methods. Also, if we want to use both P-to-P and P-to-S scattered waves to study fractures, we should search for P-to-P and P-to-S scattered waves at 'forward' and 'backward' receivers separately.

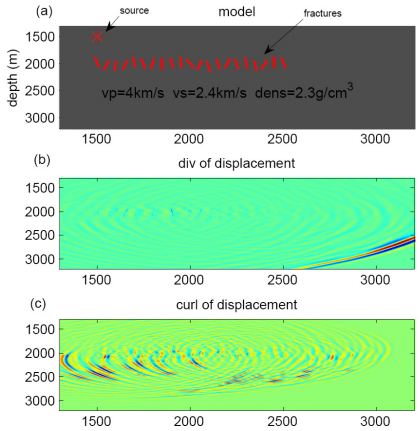

Figure 5: (a) is a homogeneous isotropic model with 21 no-parallel fractures, red lines indicate fractures and asterisk is the source. Parameters for the background medium are shown in (a) and fractures' normal and tangential compliances are $0.5x10^{-9}$m/Pa and 10^{-9}m/Pa, fracture length is 200m, the source wavelet is a Ricker wavelet with 40Hz central frequency; (b) and (c) show snapshots of the divergence and curl of the scattered wave field at 0.54s.

(2) Scattering strength

For a given frequency, scattering strength is defined as the maximum of the fracture response function over all radiation angles, so it is frequency dependent. Figure 6 shows the scattering strength of P-to-P scattering for different tangential compliance and different compliance ratios. We find that usually P-to-P scattering is stronger at small incident angle except for the case of a small compliance ratio (~0.1). Figure 7 shows the corresponding P-to-S scattering strength where regardless of the variation of compliance ratio, P-to-S scattering is always strongest near 40^0 incident angle.

By comparing P-to-P and P-to-S scattering strength in figures 6 and 7, we can find that, for most cases, P-to-S scattering is stronger than P-to-P scattering when the compliance ratio is smaller than 1. For both P-to-P and P-to-S scattering, the scattering strength will increase about 2 orders when the compliance increases 1 order, and P-to-P scattering is more sensitive to the change of normal compliance, while P-to-S scattering is more sensitive to the change of tangential compliance.

The compliance ratio is a strong function of the way the fracture surfaces interact, so this ratio may be of use for fluid identification. Both numerical simulations (Sayers, 2009; Gurevich, 2009) and laboratory measurements (Lubbe, 2008; Gurevich, 2009) suggest that the compliance ratio Z_N/Z_T should be less than 1. Based on laboratory experiment data, Lubbe (2008) suggested that a Z_N/Z_T ratio of 0.5 is probably a representative value to use in modeling studies of gas filled fractures, and the compliance ratio can

be less than 0.1 for fluid saturated fractures. Therefore, if we assume the compliance ratio Z_N/Z_T is $\leq$0.5, then, generally, P-to-S scattering would be stronger than P-to-P scattering when the incident angle is larger than 20^0. This implies that it might be easier to detect P-to-S scattered waves at the surface, although it might be hard to analyze such waves because of their complex ray paths.

We also studied the effect of matrix velocity on the fracture response functions. We find that the change of scattering patterns and scattering strength is small when the matrix velocity is changed, which implies that the fracture response functions are less sensitive to the background matrix.

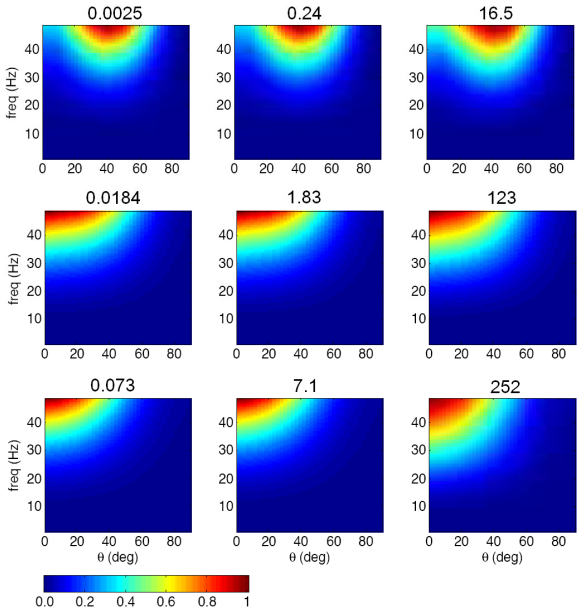

Figure 6: P-to-P scattering strength for different tangential compliance and different compliance ratio. Horizontal and vertical axes are angle of incidence and frequency. Tangential compliances are 10^{-11}m/Pa, 10^{-10}m/Pa and 10^{-9}m/Pa for the 1st, 2nd and 3rd column, respectively. And the compliance ratios are 0.1, 0.5 and 1 for the 1st, 2nd and 3rd row, respectively. The scattering strength for each panel is normalized to 1 in plotting, the number above each panel is the scaled factor (maximum scattering strength).

Conclusions

We studied scattering from single fracture using numerical modeling and found the characteristics of fracture P-to-P and P-to-S scattering, which will aid in fracture characterization. If Z_N/Z_T is $\leq$0.5, then we will detect stronger P-to-S fracture scattering energy in the field, but we need to develop more sophisticated technique to use P-to-S scattered waves for fracture characterization. In this paper, we only show the 2D study, but our work will move to 3D to see the comprehensive seismic response of a finite fracture.

Acknowledgements

This work was funded by the Eni Multiscale Reservoir Science Project within the Eni-MIT Energy Initiative Founding Member Program. Tianrun Chen was supported by an ERL Founding Member postdoctoral fellowship.

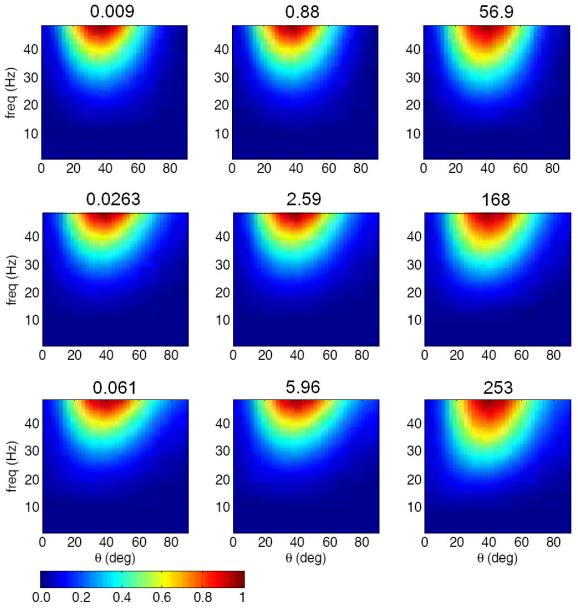

Figure 7: P-to-S scattering strength for different tangential compliance and different compliance ratio. Horizontal and vertical axes are angle of incidence and frequency.

REFERENCES

Coates, R.T. and M. Schoenberg, 1995. Finite-difference modeling of faults and fractures, *Geophysics* **60**, no. 5, 1514-1526.

Grechka, V. and M. Kachanov, 2006. Effective elasticity of fractured rocks: A snapshot of the work in progress, *Geophysics* **71**, no. 6, W45-W58.

Grechka, V., 2006. Multiple cracks in VTI rocks: Effective properties and fracture characterization, *Geophysics* **72**, no. 5, D81-D91.

Gu, B., R. Suarez-Rivera, K.T. Nihei and L.R. Myer, 1996. Incidence of plane waves upon a fracture, *J. Geophys. Res.* **101**, no. B11, 25337-25346.

Gurevich, B., D. Makarynska and M. Pervukhina, 2009. Are penny-shaped cracks a good model for compliant porosity, 79th Annual International Meeting, SEG, Expanded Abstracts, 3431-3435.

Hudson, J.A., 1991. Overall properties of heterogeneous material, *Geophys. J. Int.* **107**, 505-511.

Lubbe, R., J. Sothcott, M.H. Worthington and C. McCann, 2008. Laboratory estimates of normal and shear fracture compliance, *Geophysical Prospecting* **56**, 239-247.

Lubbe, R. and M.H. Worthington, 2006. A field investigation of fracture compliance, *Geophysical Prospecting* **54**, 319-331.

Pyrak-Nolte, L.J. and N. G.W. Cook, 1987. Elastic interface waves along a fracture, *Geophysical Research Letters* **14**, no. 11, 1107-1110.

Schoenberg, M., 1980. Elastic wave behavior across linear slip interfaces, *J. Acoust. Soc. Am.* **68**, no. 5, 1516-1521.

Schoenberg, M. and C.M. Sayers, 1995. Seismic anisotropy of fractured rock, *Geophysics* **60**, no. 1, 204-211.

Sanchez-Sesma, F.J. and U. Iturraran-Viveros, 2001. Scattering and diffraction of SH waves by a finite crack: an analytical solution, *Geophys. J. Int.* **145**, 749-758.

Sayers, C.M., 2009. Seismic characterization of reservoirs containing multiple fracture sets, *Geophysical Prospecting* **57**, 187-192.

Sayers, C.M., A.D. Taleghani and J. Adachi, 2009. The effect of mineralization on the ratio of normal to tangential compliance of fractures, *Geophysical Prospecting* **57**, 439-446.

Willis, M. E., D. Burns, R. Rao, B. Minsley, M.N. Toksoz, and L. Vetri, 2006. Spatial orientation and distribution of reservoir fractures from scattered seismic energy, *Geophysics* **71**, no. 5, O43-O51.

Worthington, M.H. and R. Lubbe, 2007. The scaling of fracture compliance, *Geological Society, London, Special Publications* **270**, 73-82.